Available online at www.sciencedirect.com

ScienceDirect

Ceramics International 40 (2014) 227–232

CERAMICS INTERNATIONAL

www.elsevier.com/locate/ceramint

Synthesis and optimization of cubic $NiFe_2O_4$ nanoparticles with enhanced saturation magnetization

Mohammad W. Kadi[a], R.M. Mohamed[a,b,*]

[a]Department of Chemistry, Faculty of Science, King Abdulaziz University, P.O. Box 80203, Jeddah 21589, Kingdom of Saudi Arabia
[b]Advanced Materials Department, Central Metallurgical R&D Institute, CMRDI, P.O. Box 87, Helwan, Cairo 11421, Egypt

Received 12 May 2013; received in revised form 30 May 2013; accepted 31 May 2013
Available online 6 June 2013

Abstract

Single phase $NiFe_2O_4$ nanoparticles were prepared via the organic acid precursor method. XRD, FTIR, SEM, and magnetization techniques were utilized to determine optimal conditions to prepare $NiFe_2O_4$ with desired properties. Calcination for 2 h at 600 °C was optimal to produce the cubic particles. The best Fe/Ni molar ratio was determined to be 2:1.1. Oxalic acid was selected as the precursor acid. Under these conditions, cubic particles with average sizes of 46 nm were obtained. A saturation magnetization value of 61.8 amu/g and a coercivity of 221.5 Oe were observed for the particles at room temperature under optimized conditions.

Keywords: A. Precursors: organic; C. Magnetic properties; D. Ferrites

1. Introduction

Ferrites have numerous industrial applications. Their importance as semiconducting magnetic materials is clearly manifested in electric and magnetic devices such as transformers, memory chips, and spintronics [1–3]. Nickel ferrite ($NiFe_2O_4$) is a soft magnetic ferrite with an inverse spinel structure. In this structure, Ni^{2+} ions occupy octahedral sites, while Fe^{3+} ions are equally distributed between octahedral and tetrahedral sites [4]. Antiparallel spin-coupling between octahedral and tetrahedral sites causes the ferromagnetic behavior of this ferrite [5]. $NiFe_2O_4$ is extensively studied because of its favorable properties such as chemical stability, high magneto-crystalline anisotropy, high electrical resistivity, chemical stability, mechanical hardness and a promise of a variety of new useful applications [6].

Morphological, dielectric, and magnetic properties for $NiFe_2O_4$ are very dependent on the preparation method and experimental conditions [4,7,8]. Many studies have reported the preparation of $NiFe_2O_4$ nanoparticles using different routes, such as hydrothermal, sol–gel, mechanical, coprecipitation, and others. For example, 20 nm irregular particles were produced by electrochemical synthesis of $NiFe_2O_4$ [6]. Nanospheres with close to the saturation magnetization of the bulk $NiFe_2O_4$ were synthesized by a reverse emulsion-assisted hydrothermal preparation [9]. Nanorods with high coercivity were synthesized by polymer-assisted coprecipitation [10]. The dependence of magnetic properties on the temperature of samples prepared by chemical coprecipitation using stable Fe and Ni salts was studied by Maaz et al. [11]. $NiFe_2O_4$ nanoparticles have also been synthesized by various methods and then coated with certain compounds to enhance specific properties of the resulting composite [12,13].

In this work, we report the preparation of highly regular cube-shaped nickel ferrite particles with the organic acid precursor method. Magnetic properties of the prepared particles were optimized based on the following factors: calcination temperatures, duration of calcination, Ni/Fe molar ratio, and the use of various organic acids in the preparation.

2. Experimental

2.1. $NiFe_2O_4$ synthesis

All of the chemicals used in this study were used as received without any further purification. Fe $(NO_3)_3 \cdot 9H_2O$ (purity 99%)

*Corresponding author at: Department of Chemistry, Faculty of Science, King Abdulaziz University, P.O. Box 80203, Jeddah 21589, Kingdom of Saudi Arabia. Tel.: +966 26 952293; fax: +966 26 952292.
E-mail address: mhmdouf@gmail.com (R.M. Mohamed).

0272-8842/$ - see front matter © 2013 Elsevier Ltd and Techna Group S.r.l. All rights reserved.
http://dx.doi.org/10.1016/j.ceramint.2013.05.128

and Ni $(NO_3)_2 \cdot 6H_2O$ (purity 98.3%) were used as iron and nickel sources. The nickel ferrite powders were synthesized with the following steps: (i) an aqueous solution of (Fe^{3+}:Ni^{2+}) ions with molar ratios of 2:1 was added to a certain amount of oxalic acid based on the stoichiometric ratios of Fe^{3+}:Ni^{2+}; (ii) the solution was stirred and evaporated at 80 °C until a clear, viscous resin was obtained; (iii) the viscous solution was dried at 110 °C for 24 h; and (iv) the dried product was calcined at a rate of 10 °C/min in static air atmosphere at temperatures ranging from 400 to 1000 °C.

2.2. Characterization

All of the prepared samples were characterized throughout the course of the analysis to deduce the optimal conditions for obtaining the best required characteristics of the produced ferrite samples. The characterization techniques used are summarized in the following points:

A. Different phases of calcined catalysts were observed using powder XRD (Bruker axis D8) employing Cu Kα radiation (λ=1.540 Å). The average crystallite size of the powders was automatically estimated from the corresponding XRD data using the Scherrer equation:

$$d = B\lambda/\beta_{1/2} \cos\ \theta$$

where d is the average particle size of the material under investigation, B is the Scherrer constant (0.89), λ is the wavelength of the X-ray beam, $\beta_{1/2}$ is the full width at half maximum of the diffraction peak and θ is the diffraction angle [14].

B. Fourier transform infrared spectroscopy (FTIR) was conducted on a Thermo Electron Magna 760 using potassium bromide (KBr) (99% purity FTIR grade, Sigma-Aldrich), in which the prepared sample powders were added to KBr in a mass ratio of 1:100 and mixed into a homogeneous solution using a shaker for 20 s prior to compressing into pellets for measurement.

C. The magnetic properties of the synthesized ferrite powders were observed using a vibrating sample magnetometer (VSM; 9600-1 LDJ, USA) at room temperature in a maximum applied field of 15 kOe. Saturation magnetization (Ms) and coercivity (Hc) were determined form the observed hysteresis loops.

D. A scanning electron microscope (JEOL JSM-6400) with an applied potential of 15 kV was used to observe the morphology of calcined samples.

2.3. Optimization methodology

After synthesis, the $NiFe_2O_4$ samples were subjected to various experimental conditions to determine those that produced optimal morphological and magnetic properties. The first of these conditions was the effect of calcination temperature. In this step, oxalic acid with a molar ratio of 1 was used as a precursor acid. Using an Fe:Ni molar ratio of 2:1 and a calcination time of 2 h, samples were calcined at 400, 600, 800, and 1000 °C at increments of 10 °C/min in static air atmosphere temperatures. The best ferrite samples were produced at 600 and 800 °C and were therefore selected for further examination of the effect of the Fe:Ni molar ratio on the final product. The best molar ratio and calcination temperature were then used to analyze the effects of calcination time. Lastly, after optimizing each of the above parameters, different organic acids were examined. Full characterization of the produced ferrite was performed at each step of the optimization process.

3. Results and discussion

3.1. Calcination temperatures

To study the effect of calcination temperature on the properties of the prepared $NiFe_2O_4$, the material was subjected

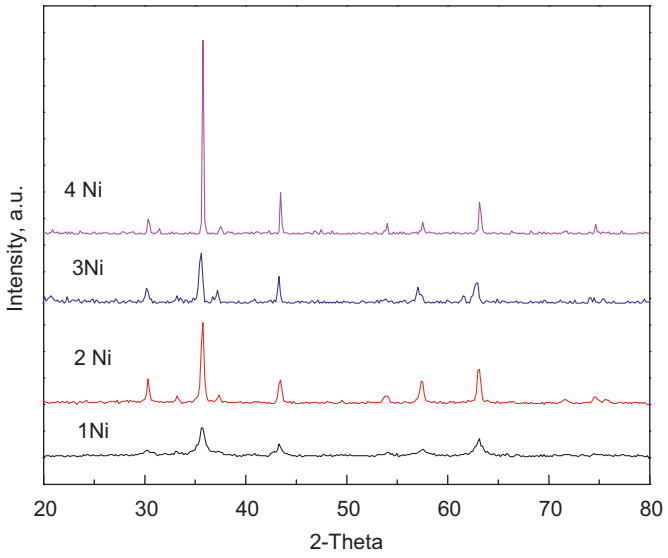

Fig. 1. XRD powder diffractograms for the calcined products.

Table 1
Applied calcination temperatures and observed properties of $NiFe_2O_4$.

Symbol of samples	Calcination temperature (°C)	Phases formed			Average particle size (nm)	Ms (emu/g)	Mr (emu/g)	Hc (Oe)
		NiO	Fe_2O_3	$NiFe_2O_4$				
1Ni	400	√	√	√	13.20	1.40	0.50	435.50
2Ni	600	√	–	√	46.40	39.20	18.50	856.80
3Ni	800	√	–	√	103.20	40.50	19.30	621.60
4Ni	1000	–	–	√	120.40	48.70	26.10	578.70

to various calcination temperatures (Table 1). An increase in the degree of crystallinity due to agglomeration of crystallites was observed with increases in the applied calcination temperature. For the most intense peak ($d=2.50574$) related to $NiFe_2O_4$ in the XRD patterns (Fig. 1), average crystallite sizes were estimated using the Debye–Scherrer formula, which showed that crystallite sizes increase with increases in calcination temperature. At 400 °C, the 1Ni calcined product produces a diffraction pattern that reflects the coexistence of three phases: NiO, Fe_2O_3 and $NiFe_2O_4$ (Table 1). The intensity of lines characterizing $NiFe_2O_4$ increased with increasing calcination temperature, indicating that $NiFe_2O_4$ is dominant at 400, 600, and 800 °C and becomes the sole phase at 1000 °C.

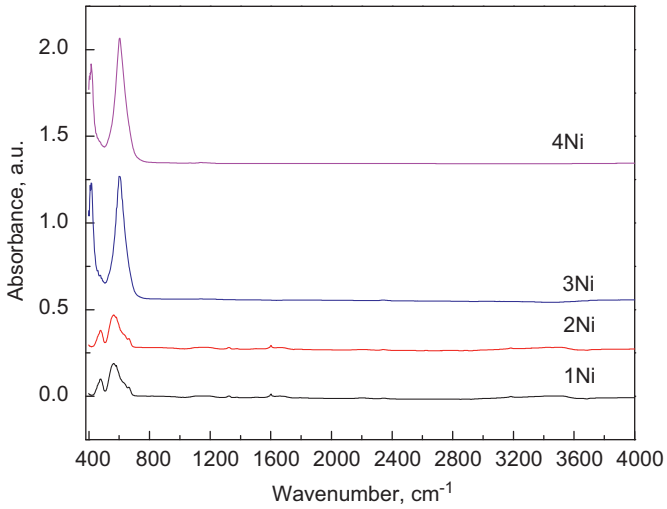

Fig. 2. FTIR spectra of the calcined products.

The chemistry of the thermal transformations of the various calcined solid thermal decomposition products of the prepared ferrite systems was studied using FTIR spectroscopy in the range of 400–4000 cm^{-1} as shown in Fig. 2. Two dominant absorption bands were observed at 575.6 cm^{-1} (υ_1) and 380–410 cm^{-1} (υ_2) due to tetrahedral Fe^{3+}–O^{2-} and octahedral pure nickel ferrite, respectively. The observed increase in sharpness of the respective FTIR bands with increased calcination temperatures indicates the increased crystallinity of existing phases. This observation was in good agreement with XRD results.

Fig. 3 shows SEM micrographs of the nickel iron oxide particles produced from their precursors calcined in the range of 400–1000 °C. It can be seen from Fig. 3a that powders produced at 400 °C showed irregular microstructures with elongated cubic-like shapes, indicating that the composition was insufficient for the complete formation of nickel hexaferrite structures. Increasing the calcination temperature to 600, 800 and 1000 °C (Fig. 3b–d) produced particles with more regular agglomeration of cube-like structures. Most of the particles were homogeneous and showed uniform structure with a narrow size distribution.

The magnetization of the produced nickel ferrite powders was performed at room temperature under an applied field of 15 kOe, and the hysteresis loops of the ferrite powders were obtained (Fig. 4). It is clear that saturation magnetization (Ms) increases with increasing calcination temperature, reaching a value of 48.7 emu/g at a calcination temperature of 1000 °C, which is smaller than the bulk value of about 55 emu/g. This result can be attributed to the formation of nanosized nickel ferrite particles with high surface areas, resulting in high surface energy and surface tension. This changes cationic preferences and leads to an increase in antisite defects, resulting in less magnetization. Moreover, the variation of the saturation magnetization with

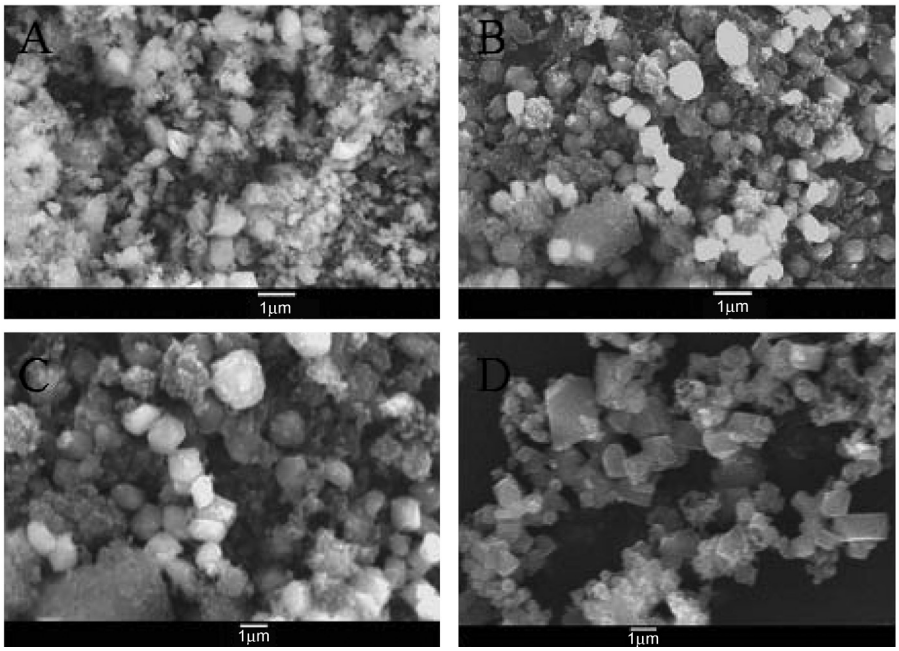

Fig. 3. SEM micrographs showing grain size and morphology of the 1Ni–4Ni systems at (A) 400 °C, (B) 600 °C, (C) 800° and (D) 1000 °C.

temperature is possibly due to changes in the degree of inversion octahedral and tetrahedral sites. Lastly, the obtained $NiFe_2O_4$ nanocrystals exhibited smaller coercivity, which should be attributed to their nanostructures.

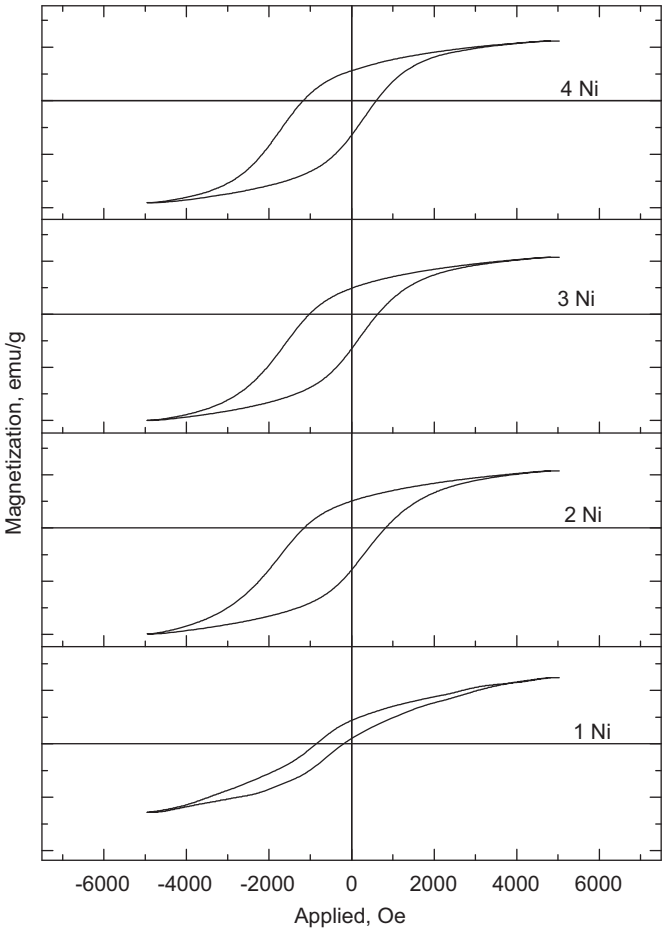

Fig. 4. Effect of calcination temperature on the *M–H* hysteresis loop of the systems under investigation.

3.2. Fe:Ni molar ratio

It is evident from Section 2 that calcination at 600 and 800 °C produces the best properties of $NiFe_2O_4$. Taking this result into consideration, the effects of changing the molar ratio of Fe and Ni in the preparation process were studied. Tables 2 and 3 summarize the effects of the Fe:Ni molar ratio on the properties of prepared ferrites at 600 and 800 °C. From XRD spectra, one can observe that both NiO and Fe_2O_3 phases begin to disappear, thereby leaving $NiFe_2O_4$ as the sole phase in the prepared ferrite at higher Fe:Ni molar ratios. The 6Ni system appears to be the best system with regards to magnetization, particle size and morphological properties. This is evident from the high saturation magnetization value of 61.8 emu/g, the presence of only $NiFe_2O_4$, and the perfect cubic particles, as shown in Figs. 5 and 6. Therefore, a molar Fe:Ni ratio of 2:1.1 was adopted as the optimal ratio for the preparation of nickel ferrite particles with the desired magnetic and morphological properties.

3.3. Effect of calcination time

Calcination times of 0.5, 1.0, and 2 h were examined under optimal experimental conditions deduced from Sections 3.1 and 3.2. A summary of observed properties is presented in Table 4. There is a significant increase in magnetization with increase in calcination time. Two hours of calcination also allows for the formation of unified cubic particles, while calcination for lesser times yields irregular shapes with large agglomerations, as can be seen from SEM micrographs.

3.4. Effect of precursor acid type

Tartaric, citric, and oxalic acids were used as precursor acids for the preparation of $NiFe_2O_4$ under the optimal experimental conditions determined in the analyses described in previous sections. Based on XRD patterns, it was clear that citric acid

Table 2
Observed properties of prepared ferrites using various Fe:Ni molar ratios at 600 °C.

Symbol of samples	Fe:Ni molar ratio	Phases formed			Ms (emu/g)	Mr (emu/g)	Hc (Oe)
		NiO	Fe_2O_3	$NiFe_2O_4$			
2Ni	2:1	–	√	√	39.2	18.5	856.8
5Ni	2:1.05	–	√	√	43.2	25.5	726.7
6Ni	2:1.1	–	–	√	61.8	41.5	221.5
7Ni	2:1.15	–	–	√	50.9	29.9	590.2

Table 3
Observed properties of prepared ferrites using various Fe:Ni molar ratios at 800 °C.

Symbol of samples	Fe:Ni molar ratio	Phases formed			Ms (emu/g)	Mr (emu/g)	Hc (Oe)
		NiO	Fe_2O_3	$NiFe_2O_4$			
3Ni	2:1	–	√	√	40.5	19.3	621.6
8Ni	2:1.05	–	–	√	54.0	32.4	446.9
9Ni	2:1.1	–	–	√	50.2	29.3	541.0
10Ni	2:1.15	–	–	Sole	57.4	34.4	403.8

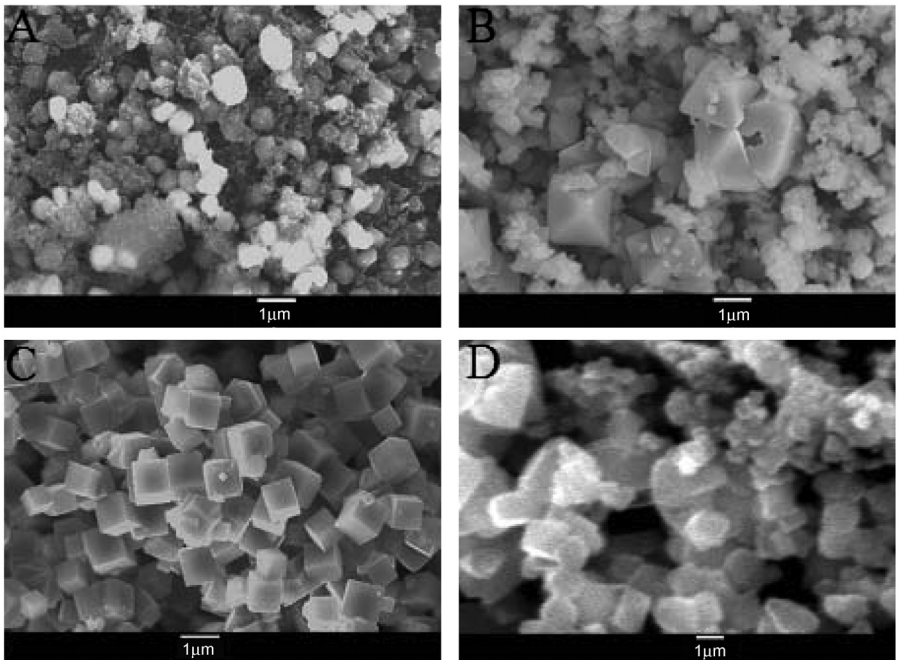

Fig. 5. SEM micrographs showing grain size and morphology of 2Ni (A), 5Ni (B), 6Ni (C) and 7Ni (D).

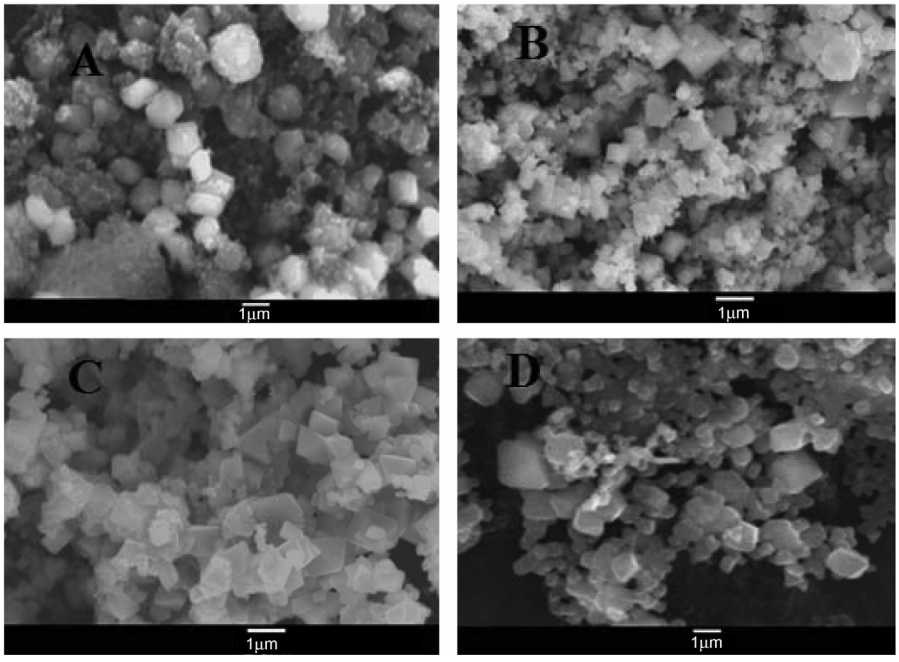

Fig. 6. SEM micrographs showing grain size and morphology of 3Ni (A), 8Ni (B), 9Ni (C) and 10Ni (D).

and tartaric acid produced $NiFe_2O_4$ that coexisted with species of rhombohedral iron oxide Fe_2O_3 and NiO phases. The examination of *M–H* hysteresis loops revealed that magnetization with either citric acid or tartaric acid was significantly smaller (34 and 25 amu/g) than oxalic acid (62 amu/g). The particles that were prepared using citric acid and tartaric acid were spherical, with some irregularly shaped particles. Nikolić et al. reported spherical particles with average sizes of 18 nm using citric acid as a precursor. These authors found little effect on the product when tartaric acid and malonic acid were used [16].

3.5. Comparison to other methods of synthesis

It is evident from the application of various experimental conditions that properties of synthesized particles are extremely dependent on the preparation process. If fact, a survey of

Table 4
Observed properties of prepared ferrites calcined for various times at 600 °C.

Symbol of samples	Calcination time (h)	Phases formed			Ms (emu/g)	Mr (emu/g)	Hc (Oe)
		NiO	Fe_2O_3	$NiFe_2O_4$			
11Ni	0.5	–	√	√	19.00	1.20	1721.00
12Ni	1.00	–	√	√	37.00	7.50	948.70
6Ni	2.00	–	–	√	62.00	41.50	222.00

literature shows that a change in preparation methodology and conditions can produce particles that completely differ in character. Experimentally, one can take advantage of various preparation techniques to produce particles that possess certain characteristics designed for a specific application. Supporting materials S_1 summarizes certain properties of particles synthesized by various methods [15,6,10,9] and this work. Wide differences in morphologies, magnetic properties, and particle sizes are apparent for these particles.

4. Conclusions

Nickel ferrite nanoparticles have been successfully synthesized using an oxalic acid precursor method. Crystalline cubic structures were formed that consisted of only a single phase of $NiFe_2O_4$. Optimal experimental conditions were determined through extensive characterization using XRD, FTIR, SEM, and magnetization. Optimal experimental conditions are as follows: calcination temperature of 600 °C, calcination time of 2 h, Fe/Ni molar ratio of 2:1.1, and the use of oxalic acid as a precursor acid. Under these conditions, good saturation magnetization (62.00 emu/g) was achieved.

Appendix A. Supporting information

Supplementary data associated with this article can be found in the online version at http://dx.doi.org/10.1016/j.ceramint.2013.05.128.

References

[1] K. Kamala Bharathi, M. Noor-A-Alam, R.S. Vemuri, C.V. Ramana, Correlation between microstructure, electrical and optical properties of nanocrystalline $NiFe_{1.925}Dy_{0.075}O_4$ thin films, RSC Advances 2 (2012) 941–948.
[2] K. Kamala Bharathi, G. Markandeyulu, C.V. Ramana, Impedance spectroscopic characterization of Sm and Ho doped Ni ferrites, Journal of the Electrochemical Society 158 (2011) G71–G78.
[3] K. Kamala Bharathi, G. Markandeyulu, C.V. Ramana, Structural, magnetic, electrical, and magnetoelectric properties of Sm- and Ho- substituted nickel ferrites, Journal of Physical Chemistry C115 (2011) 554–560.
[4] T.F. Marinca, I. Chicinas, O. Isnard, V. Pop, F. Popa, Synthesis, structural and magnetic characterization of nanocrystalline nickel ferrite-$NiFe_2O_4$ obtained by reactive milling, Journal of Alloys and Compounds 509 (2011) 7931–7936.
[5] B.D. Cullity, C.D. Graham, Introduction to Magnetic Materials, second ed., Wiley, 2009, p. 194.
[6] R. Galindo, E. Mazario, S. Gutiérrez, M.P. Morales, P. Herrasti, Electrochemical synthesis of $NiFe_2O_4$ nanoparticles: characterization and their catalytic applications, Journal of Alloys and Compounds 536S (2012) S241–S244.
[7] K. Sudalai Muthu, N. Lakshminarasimhan, Impedance spectroscopicstudieson $NiFe_2O_4$ with different morphologies: microstructure vs. dielectric properties, Ceramics International 39 (2013) 2309–2315.
[8] C. Cheng, Enhanced magnetization and conductive phase in $NiFe_2O_4$, Journal of Magnetism and Magnetic Materials 325 (2013) 144–146.
[9] J. Zhang, J. Shi, M. Gong, Synthesis of magnetic nickel spinel ferrite nanospheres by a reverse emulsion-assisted hydrothermal process, Journal of Solid State Chemistry 182 (2009) 2135–2140.
[10] P. Sivakumar, R. Ramesh, A. Ramanand, S. Ponnusamy, C. Muthamizhchelvan, Synthesis and characterization of $NiFe_2O_4$ nanoparticles and nanorods, Journal of Alloys and Compounds 563 (2013) 6–11.
[11] K. Maaz, A. Mumtaz, S.K. Hasanain, M.F. Bertino, Temperature dependent coercivity and magnetization of nickel ferrite nanoparticles, Journal of Magnetism and Magnetic Materials 322 (2010) 2199–2202.
[12] M.R. Phadatare, V.M. Khot, A.B. Salunkhe, N.D. Thorat, S.H. Pawar, Studies on polyethylene glycol coating on $NiFe_2O_4$ nanoparticles for biomedical applications, Journal of Magnetism and Magnetic Materials 324 (2012) 770–772.
[13] A. Tomitaka, T. Koshi, S. Hatsugai, T. Yamada, Y. Takemura, Magnetic characterization of surface-coated magnetic nanoparticles for biomedical application, Journal of Magnetism and Magnetic Materials 323 (2011) 1398–1403.
[14] P. Tyagi, A.G. Vedeshwar, Grain size dependent optical band gap of CdI_2 films, Bulletin of Materials Science 24 (2001) 297.
[15] L. Sonali, S.S. Darshane, S.L. Suryavanshi, S. Mulla, Nanostructured nickel ferrite: a liquid petroleum gas sensor, Ceramics International 35 (2009) 1793–1797.
[16] A.S. Nikolić, N. Jović, J. Rogan, A. Kremenović, M. Ristić, A. Meden, B. Antic, Carboxylic acids and polyethylene glycol assisted synthesis of nanocrystalline nickel ferrites, Ceramics International 39 (2013) 6681–6688.